Methane Steam Reforming: II. Diffusional Limitations and Reactor Simulation

Given the intrinsic kinetics, the tortuosity factor of a $Ni/MgAl_2O_4$ catalyst was determined under reaction conditions by minimizing the sum of squares of residuals of the experimental and the simulated conversions. The parallel cross-linked pore model with uncorrelated pore size distribution and orientation was used in the calculation of the effective diffusivities. A modified collocation method was used to obtain the partial pressure profiles of the reacting components in the catalyst pellet. The simulation of the experimental reactor during the optimization of the tortuosity factor also yielded the effectiveness factors of the reactions. The results of the simulation of an industrial steam reformer are also discussed.

Jianguo Xu
Gilbert F. Froment
Laboratorium voor
Petrochemische Techniek
Rijksuniversiteit Gent
Gent, Belgium

Introduction

In Part I of this paper, the intrinsic kinetics of the reactions occurring in the steam reformation of methane were determined. The application of these kinetic equations in the simulation of a commercial reformer, in which large catalyst particles are used, requires the diffusional limitations to be accounted for. In the present paper, these are first experimentally studied and related to the tortuosity factor, a characteristic of the pore network of the catalyst. Then, this information is combined with the intrinsic kinetics to simulate an industrial steam reformer.

Tortuosity Factor of a Steam Reforming Catalyst

Effective diffusivities and tortuosity factor

The diffusivities of the reacting components $A, \ldots$ are related to the molecular and Knudsen diffusivities by:

$$\frac{1}{D_A(r_i)} = \frac{1}{D_{mA}} + \frac{1}{D_{kA}(r_i)} \tag{1}$$

The pore size distribution of the steam reforming catalyst was measured by mercury penetration and nitrogen desorption. It is presented in Table 1. Given this distribution, an average value $\bar{D}_A$ can be calculated from:

$$\bar{D}_A = \int_0^R D_A(r_i) \cdot f(r_i)\, dr \tag{2}$$

or rather from:

$$\bar{D}_A = \sum_i D_A(r_i) \cdot S(r_i) \tag{3}$$

where $S(r_i)$ is the void volume fraction taken by the pores with radii between r_i and r_{i+1}:

$$S(r_i) = \frac{V_{g,i}}{\sum_i V_{g,i}} = \frac{V_{g,i}}{V_g} \tag{4}$$

Table 1. Pore Size Distribution of Catalyst

Pore Dia. Å	Δ Vol. of Voids ΔV_g, cm³/g
30	0.0040
30-50	0.0250
50-80	0.0262
80-120	0.0379
120-200	0.0573
200-500	0.0388
500-1,000	0.0190
1,000-10,000	0.0290
10,000-100,000	0.0136
Sum	0.2508

With this average, $\bar{D}_A$, an effective diffusivity is calculated from the relation:

$$D_{eA} = \frac{\epsilon_s}{\tau} \bar{D}_A \tag{5}$$

The tortuosity factor τ is the simplified and lumped effect of many complexities. Tortuosity factors ranging from 1.5 up to 10 or more have been reported. Model predictions lead to values of the tortuosity factor of $1/\epsilon_s$ according to Wakao and Smith (1962), of 2 with the parallel-path pore model (Wheeler, 1951), of 3 with the parallel cross-linked pore model (Feng and Stewart, 1973), or of 4 when using the random pore model (Beeckman and Froment, 1982). De Deken et al. (1982) obtained a value of about 4.7 by the gas chromatographic technique by applying the van Deemter equation (Van Deemter et al., 1956) and using the average pore diameter in calculating the Knudsen diffusivities. Dumez and Froment (1976) found a value of 5 using Eq. 2 and the mass balance equation considering both diffusion and reaction. They fitted the experimental results obtained in a differential reactor and used the macropore radius as the r value in calculating the Knudsen diffusivities, since the micropores were so short that no diffusional resistance occurred in them. Since the tortuosity factors obtained by different authors cover such a wide range, it is preferable, at this stage, to measure τ for the catalyst under consideration.

The experimental determination of the tortuosity factor is done in two ways.

1. The purely physical method, which does not require the knowledge of the intrinsic kinetics of the reaction, but which has the drawback that the conditions for determination may be far away from the reaction conditions.

2. The method that determines τ under reaction conditions—the approach used in the present paper. Combination of the intrinsic kinetics and the diffusion aspects permits the simulation of the reactor, in which diffusional limitations occur. Fitting the calculated results to the experimental ones permits τ to be determined. Because a certain deactivation of the catalyst was observed under steam reforming conditions, τ was determined under conditions of reverse water gas shift.

Reverse water-gas shift experiments

For the details of the reactor, see Part I.

The commercial catalyst used is a nickel catalyst supported on $MgAl_2O_4$, the core of which is completely inert. The catalyst rings were crushed into 1.0–1.2 mm particles. The particles without nickel were eliminated from the sample by magnetic separation. A catalyst sample of 0.4 g was diluted with inert α alumina.

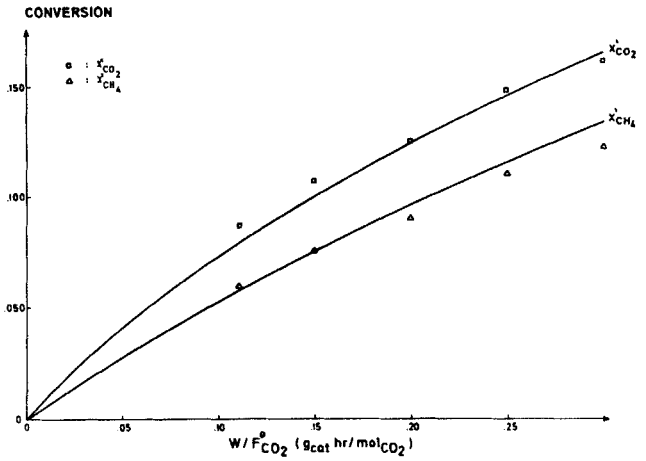

Figure 1. Reverse of water gas shift.
Experimental (□, △) and simulated (curves) conversions in the presence of diffusional limitations: T = 400°C; p_t = 3.0 × 10⁵ Pa; H_2/CO_2 molar feed ratio = 1.0; and d_p = 1.1 mm

The reactor was heated in a hydrogen stream under atmospheric pressure. The heating rate was 2°C/min. The temperature was maintained at 810°C for 12 hours after it reached that value, still in a hydrogen stream at atmospheric pressure. The temperature was reduced in a hydrogen stream to 400°C. When the temperature reached 400°C, the back pressure of the reactor was raised to 3 bar. Then, the hydrogen flow rate was raised to 1.6 mol/h and the CO_2 flow was switched on, also at 1.6 mol/h. Carbon monoxide and CH_4 were formed via the reverse of the water-gas shift and methanation reactions. The above conditions were kept for 24 hours to confirm that the activity level of the catalyst was stable. Then, the experiments at different $W/F^o_{CO_2}$ values were carried out. The pressure, temperature, and H_2/CO_2 feed ratio were kept at 3 bar, 400°C and 1 mol H_2/mol CO_2. The reactor effluent was analyzed by gas chromatography. Since no significant carbon deposition occurred, the total conversion of CO_2 and the conversion of CO_2 into CH_4 completely describe the composition of the effluent gas. The results are shown in Figure 1.

Estimation of the tortuosity factor

Even when CO_2 and H_2 are fed and the temperature is kept at 400°C, methanation cannot be avoided, so that the continuity equations for two key components have to be integrated to obtain the concentration gradients inside the catalyst particle, considered to be spherical:

$$\frac{1}{\xi^2}\frac{d}{d\xi}\left(D_{e,CO_2}\,\xi^2\,\frac{dp_{s,CO_2}}{d\xi}\right) = 10^{-2}RT \cdot R_p^2 \cdot r'_{CO_2}(P_s)\rho_s \tag{6a}$$

$$\frac{1}{\xi^2}\frac{d}{d\xi}\left(D_{e,CH_4}\,\xi^2\,\frac{dp_{s,CH_4}}{d\xi}\right) = 10^{-2}RT \cdot R_p^2 \cdot r'_{CH_4}(P_s)\rho_s \tag{6b}$$

with $P_s = (p_{s,CO_2}; p_{s,CH_4}; p_{s,H_2}; p_{s,CO}; p_{s,H_2O})^T$

Boundary conditions:

$$dp_{s,CO_2}/d\xi = dp_{s,CH_4}/d\xi = 0 \quad \text{at } \xi = 0 \tag{6c}$$

$$p_{s,CO_2} = p_{CO_2},\ p_{s,CH_4} = p_{CH_4} \quad \text{at } \xi = 1 \tag{6d}$$

The profiles of the dependent components are obtained from the algebraic equations:

$$p_{s,CO} - p_{CO} = (D_{e,CO_2}/D_{e,CO})(p_{CO_2} - p_{s,CO_2}) - (D_{e,CH_4}/D_{e,CO})(p_{s,CH_4} - p_{CH_4}) \tag{6e}$$

$$p_{s,H_2O} - p_{H_2O} = (D_{e,CO_2}/D_{e,H_2O})(p_{CO_2} - p_{s,CO_2}) + (D_{e,CH_4}/D_{e,H_2O})(p_{s,CH_4} - p_{CH_4}) \tag{6f}$$

$$p_{s,H_2} - p_{H_2} = (D_{e,CO_2}/D_{H_2})(p_{s,CO_2} - p_{CO_2}) - (3D_{e,CH_4}/D_{e,H_2})(p_{s,CH_4} - p_{CH_4}) \tag{6g}$$

The rate equations were given in Part I.

The global spline orthogonal collocation method was used in solving the coupled differential equations. A modified iteration algorithm which strongly reduces the computation time of the collocation method was developed and will be published later.

After the concentration profiles are calculated, the actual, observed rates can be obtained. The actual rates at a certain reactor coordinate (or certain $W/F^o_{CO_2}$ value) can be calculated according to Eq. 7:

$$(r_j)_{obs} = \int_0^V r_j(P_s)\frac{dV}{V} \tag{7}$$

The D_{ej} values were calculated from Eq. 5, with the tortuosity to be determined. The molecular diffusivities were calculated by Eq. (3.2.c-7) given in Froment and Bischoff (1979), while the binary diffusivities used in this formula were obtained from the Wilke-Chang equation (1955).

One way to determine τ is to match the calculated $(r'_{CH_4})_{obs}$ and $(r'_{CO_2})_{obs}$ to the experimental values by optimizing the τ value. Since an integral reactor was used in the present work, the integral method of kinetic analysis was applied. This requires the residual sum of squares $\Sigma(x_j - \hat{x}_j)^2$ to be minimized by optimizing τ. The fluid-phase continuity equations for CO_2 and CH_4 are:

$$dx'_{CO_2}/d(W/F^o_{CO_2}) = (r'_{CO_2})_{obs}$$
$$dx'_{CH_4}/d(W/F^o_{CO_2}) = (r'_{CH_4})_{obs} \tag{8}$$

with

$$x'_{CH_4} = x'_{CO_2} = 0 \quad \text{at } W/F^o_{CO_2} = 0$$

They were integrated by means of a Runge-Kutta routine. The conversions x'_{CH_4} and x'_{CO_2} are the conversion of CO_2 into CH_4 and the total conversion of CO_2. The rates $(r'_{CO_2})_{obs}$ and $(r'_{CH_4})_{obs}$ are those obtained through Eq. 7. In each node used in the numerical integration of Eq. 8, the set of second-order differential equations (Eqs. 6a–6b) also had to be integrated.

The simulated conversions are plotted in Figure 1, together with the experimental ones.

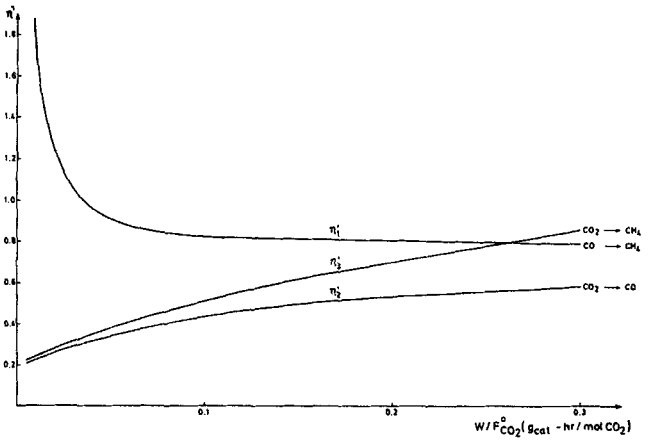

Figure 2. Reverse of water gas shift.
Evolution of effectiveness factors: $T = 400°C$; $p_t = 3.0$ bar; H_2/CO_2 molar feed ratio = 1.0; and $d_p = 1.1$ mm

Minimizing the sum of squares of residuals of the calculated conversions and the experimental ones yielded a τ value of 3.54.

Figure 2 shows the evolution of the effectiveness factors with $W/F^o_{CO_2}$.

The effectiveness factor η_i was calculated from:

$$\eta_i = \frac{\int_0^V r_i(P_s)\rho_s \frac{dV}{V}}{r_i(P^s_s)\rho_s} \tag{9}$$

It can be seen that η'_1, the effectiveness factor for the reverse of reaction I (*viz.* Table 2 of Part I) exceeds 1 in the upper part of the reactor. This is not surprising, since the reaction is consecutive to the reverse of the water-gas shift. Further down in the bed, where more CO is present, the CO gradient inside the particle reverses. This, together with the profile of the other reactant and feed component, H_2, which also decreases from the surface toward the center of the particle, leads to values of η'_1 which become smaller than one. The effectiveness factor of the reverse of the water-gas shift, η'_2, is smaller than one and continuously increases with $W/F^o_{CO_2}$, i.e., with x_{CO_2}. The effectiveness factor of the methanation, the reverse of reaction III (*viz.* Table 2 of Part I), also behaves in the usual way.

Simulation of an Industrial Steam Reformer

The conditions used in the simulation of an industrial steam reformer are similar to those dealt with previously by De Deken et al. (1982). They are listed in Table 2.

The one-dimensional heterogeneous model was used (Froment and Bischoff, 1979). The equations are:

Continuity equations for CH_4 and CO_2:

$$\frac{dx_{CH_4}}{dz} = \Omega\rho_B\eta_{CH_4}r_{CH_4}/F^o_{CH_4} \tag{10a}$$

$$\frac{dx_{CO_2}}{dz} = \Omega\rho_B\eta_{CO_2}r_{CO_2}/F^o_{CH_4} \tag{10b}$$

Table 2. Input Data for the Simulation of a Commercial Reformer

T_o = 793.15 K
p_{to} = 29 bar
Feed per tube
135.00 Nm^3/h natural gas
399.17 Nm^3/h steam
Natural gas composition
CH_4 = 81.5 vol. %
N_2 = 14.1
C_2H_6 = 2.8
CO_2 = 1.0
C_3H_8 = 0.4
C_4H_{10} = 0.1
C_5H_{12} = 0.2
Equiv. CH_4 feed = 5.168 kmol/h
Molar ratio H_2O/CH_4 = 3.358
CO_2/CH_4 = 0.056
H_2/CH_4 = 0.122
N_2/CH_4 = 0.164
Internal tube dia. = 0.1016 m
External tube dia. = 0.1322 m
Total tube length = 12 m
Heated tube length = 11.12 m
Dimensions of catalyst ring
d_{pe} = 0.0173 m
d_{pi} = 0.0084 m
H = 0.010 m
ρ_s = 2,355.2 kg/m^3
Thickness of active layer = 0.002 m

Energy equation:

$$\frac{dT}{dz} = \frac{1}{c_p \rho_g u_s}\left[\rho_B \Sigma(-\Delta H_i) r_i \eta_i - 4\frac{U}{d_{ti}}(T - T_r)\right] \quad (10c)$$

Momentum equation:

$$-\frac{dp_t}{dz} = \frac{f\rho_g u_s^2}{g d_p} \quad (10d)$$

with $x_{CH_4} = x_{CO_2}$; $T = T_o$; $p_t = (p_t)_o$ at $z = 0$.

The heat transfer coefficient U is calculated from:

$$\frac{1}{U} = \frac{d_{ti}}{2\lambda_{st}} \ln\left(\frac{d_{te}}{d_{ti}}\right) + \frac{1}{\alpha_i} \quad (11)$$

To predict as closely as possible by means of the above one-dimensional model, the cross-sectional averaged conversions and temperatures that would be calculated by a two-dimensional model α_i is related to the heat transfer parameters of the two-dimensional model by means of the following formula (Froment and Bischoff, 1979):

$$\alpha_i = \frac{8\lambda_{er}\alpha_w}{8\lambda_{er} + \alpha_w d_{ti}} \quad (12)$$

where

$$\alpha_w = \alpha_w^o + 0.444\, Re\, Pr \frac{\lambda_g}{d_p}$$

$$\lambda_{er} = \lambda_{er}^o + 0.14\, \lambda_g Re\, Pr$$

with α_w^o calculated from (De Wasch and Froment, 1972):

$$\alpha_w^o = \frac{8.694}{(d_{ti})^{4/3}} \lambda_{er}^o$$

and λ_{er}^o from the relation introduced by Kunii and Smith (1960).

The friction factor in Eq. 10d is that of Ergun (1952). The equivalent diameter of the catalyst rings is calculated according to Brauer (1957) and the porosity of the bed according to Reichelt and Blasz (1971).

Since the partial pressure gradients are limited to a very thin layer near the surface, planar geometry was used. The continuity equations for CH_4 and CO_2 then become:

$$D_{e,CH_4}\frac{d^2 p_{s,CH_4}}{d\xi^2} = 10^{-2} RT \cdot R_p^2 \cdot r_{CH_4}(P_s)\rho_s \quad (13a)$$

$$D_{e,CO_2}\frac{d^2 p_{s,CO_2}}{d\xi^2} = 10^{-2} RT \cdot R_p^2 \cdot r_{CO_2}(P_s)\rho_s \quad (13b)$$

with the boundary and other equations as in Eqs. 6c to 6g and R_p here the half width of the slab.

The effectiveness factors were calculated from Eq. 7, using spline orthogonal collocation to calculate the concentration profiles. Three splines were used, with zero reaction rate in the innermost. The two splines, in which the concentration gradients occur, have a total thickness of 0.08 mm. The spline point was positioned at the dimensionless coordinate of 0.7, with 14 collocation points in the outer and eight in the inner of the splines.

The industrial catalyst is ring-shaped, with active layers at the external and internal surface of 2 mm. The slab upon which the calculation of the effectiveness factor was based, was chosen to contain the same amount of active material, therefore the same volume as the active part of the ring. This active volume-equivalent slab has an external surface per unit volume (a_v or $a_m\rho_s$) which is easily calculated to be 1.071 times that of the active part of the ring, for the dimensions given in Table 2. Therefore, the η calculated on the basis of the active volume-equivalent slab has to be divided by this factor to obtain the value for the industrial ring-shaped catalyst. The temperature of the external reactor wall is generated from a coupled simulation of the fire box and the reactor. A zone model, developed by Rao et al. (1988) for the simulation of the temperature distribution in an ethylene furnace, was adapted to the reformer furnace. The results of the simulation are shown in Figures 3 to 7.

The evolution of the total conversion of methane and of the conversion of methane into CO_2 is shown in Figure 3, together with the process gas temperature, total pressure and wall temperature profiles. The temperature drop over the film surrounding the catalyst particle is negligible, as shown already by De Deken et al. (1982).

The profiles of the intrinsic rates in the reactor are shown in Figure 4. The intrinsic rate r_2 changes from positive to negative at a reactor length of about 4 m.

The approach to equilibrium of the reactions, defined by:

$$V(i) = \left(\prod_j p_j^{\nu_j}\right)_i \Big/ K_i \quad (14)$$

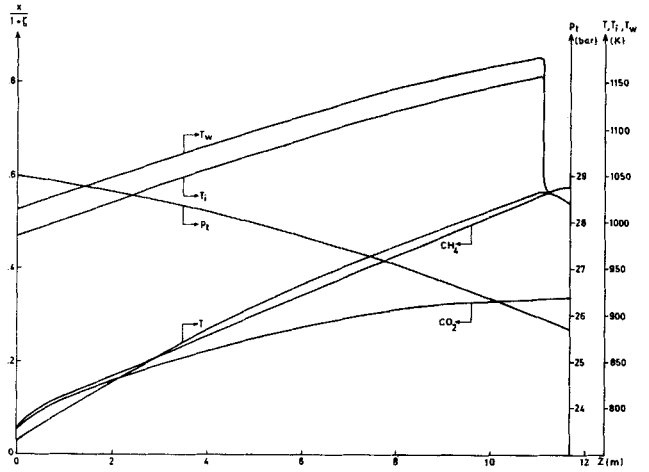

Figure 3. Evolution of conversions, total pressure, process gas and external and internal tube skin temperature in a commercial steam reformer.

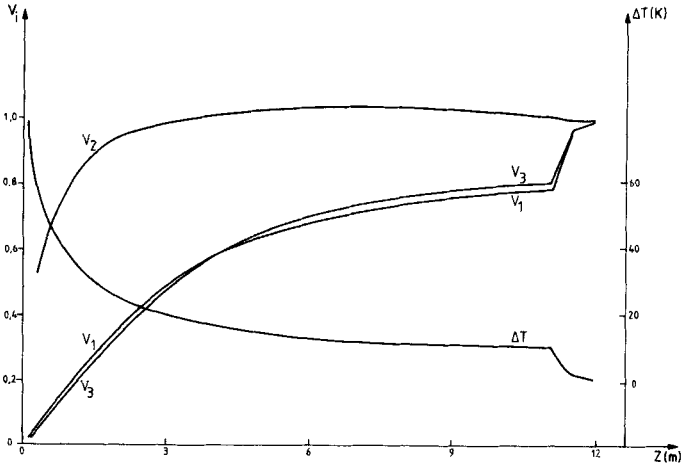

Figure 5. Approach to equilibrium in a commercial steam reformer.

$V(1)$: $CH_4 + H_2O \rightleftharpoons CO + 3H_2$ (reaction I of Part I)
$V(2)$: $CO + H_2O \rightleftharpoons CO_2 + H_2$ (reaction II)
$V(3)$: $CH_4 + 2H_2O \rightleftharpoons CO_2 + 4H_2$ (reaction III)

is shown in Figure 5. Beyond 3 m already, reaction II (*viz.* Table 2 of Part I) comes very close to equilibrium. For reactions I and III, the approach to equilibrium exceeds 70% in the second half of the reactor. It only slowly increases to 80% because the rising process gas temperature shifts the equilibrium of these reactions further to the right. The conversion in a steam reformer is limited mainly by the heat flux supplied per unit weight of catalyst.

Figure 5 also shows ΔT, the local difference between the actual process gas temperature and the temperature that would be reached if the process gas were at equilibrium. This ΔT is often used to characterize the operation of an industrial reformer. Its value is about 10°C at the end of the heated part of the tube.

The evolution of the various effectiveness factors is shown in Figure 6. The effectiveness factor of reaction II shows a discontinuity at a reactor length of 3.4 m, because the direction of reaction II changes from positive to negative on the catalyst surface, while there is no such tendency yet inside the catalyst particle. The η_2 value switches back from negative to positive values at a reactor length of 9 m only, meaning that the overall effect of the reaction inside the catalyst pellet reverses from the formation of CO_2 and H_2 out of CO and H_2O to the formation of CO and H_2O out of CO_2 and H_2.

The effectiveness factors of reactions I and III both decrease through the reactor, despite the decrease of the rate of reaction III. When the reaction is near equilibrium, the reaction rate is even more sensitive with respect to changes in concentration, since the rate of the reverse reaction increases with a similar value as the reduction in rate of the forward reaction. The values of the effectiveness factors η_1 and η_3 obtained in the present study are close to those calculated by De Deken et al. (1982) for a different catalyst. These low effectiveness factors also explain why many authors obtained activation energies for steam reforming of approximately half the intrinsic values. The partial pressures of the catalyst surface components are very close to the equilibrium values at reactor lengths exceeding 6 m. In spite of this, the reaction rates do not drop to very small values, because of the temperature rise which shifts the equilibrium to

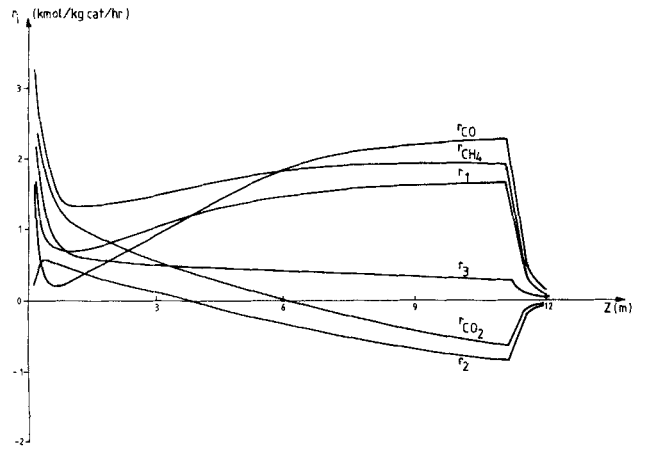

Figure 4. Evolution of intrinsic reaction rates in a commercial steam reformer.

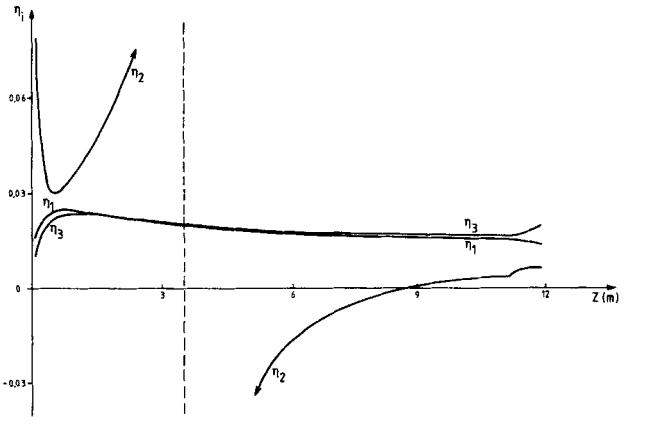

Figure 6. Evolution of effectiveness factors in a commercial steam reformer.

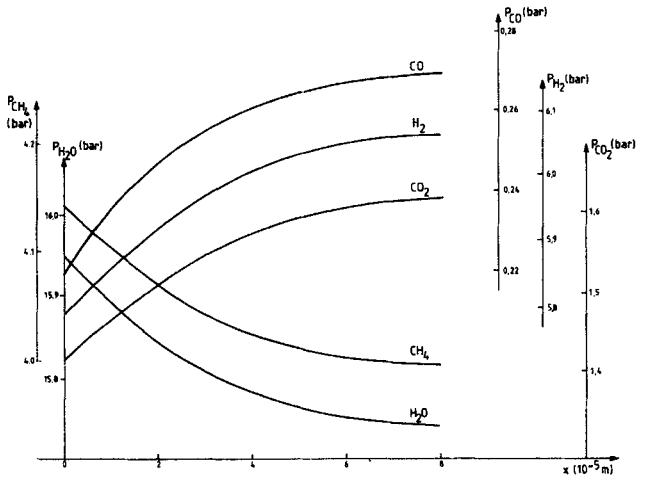

Figure 7. Partial pressure profiles in the catalyst pellet at $Z = 4.00$ m from the inlet in a commercial steam reformer tube.

the right. The partial pressure profiles in the catalyst pellet at a reactor length of 4.00 m are shown in Figure 7.

Acknowledgment

The pore size distribution was measured by Dr. Cahen, Labofina, Feluy, Belgium. J. Xu is grateful to Commissariaat-Generaal voor de Internationale Culturele Samenwerking van de Vlaamse Gemeenschap for the financial support during the work.

Notation

a_m = surface area of the catalyst pellet per kg cat, m^2/kg cat
c_i = concentration of component i in gas phase, kmol/m^3
c_p = heat capacity of the process gas, kJ/(kg · K)
C_s = vector of $c_{s,i}$
$c_{s,i}$ = concentration of component i inside catalyst pellet, kmol/m^3
D_A = diffusivity of component A, m^2/h
D_{eA} = effective diffusivity of component A, m^2/h
D_{mA} = molecular diffusivity of component A, m^2/h
D_{KA} = Knudsen diffusivity of component A, m^2/h
d_p = diameter of the catalyst pellet, m
d_{pe} = external diameter of catalyst ring, m
d_{pi} = inner diameter of the catalyst ring, m
d_{te} = external diameter of the reactor, tube, m
d_{ti} = inner diameter of the reactor tube, m
$F^o_{CH_4}$ = molar flow rate of CH_4 in the feed, kmol/h
$F^o_{CO_2}$ = molar flow rate of CO_2 in the feed, kmol/h
f = friction factor in the momentum equation
$f(r)$ = fraction of pores with radius r
g = acceleration of gravity, m/h^2
H = height of the catalyst ring, m
ΔH_i = enthalpy change of reaction i, kJ/kmol
K_i = equilibrium constant of reactions I, II, III, bar^2, –, bar^2
K_j = adsorption constant for component j,
j = CO, H_2, CH_4, bar^{-1}
j = H_2O
k_i = rate coefficient of reaction i,
i = I, III, kmol · bar$^{0.5}$/(kg cat · h)
i = II, kmol/(kg cat · h · bar)
l = thickness of the active part on each side of the catalyst ring, m
pi = partial pressure of component i, bar
p_t = total pressure, bar
R = gas constant, kJ/(kmol · K)
R_p = equivalent radius of the catalyst particle, m
r_{CH_4} = total rate of disappearance of CH_4 in steam reforming, kmol CH_4/(kg cat · h)
r'_{CH_4} = rate of formation of CH_4 in reverse of water gas shift, kmol CH_4/(kg cat · h)
r_{CO_2} = rate of conversion of CH_4 into CO_2 in steam reforming, kmol CH_4/(kg cat · h)
r'_{CO_2} = rate of disappearance of CO_2 in reverse of water gas shift, kmol CO_2/(kg cat · h)
r = pore radius, m or Å
S = volume fraction of pores with radius $r_i < r < r_{i+1}$
T = process gas temperature, K
T_i = internal tube skin temperature, K
T_w = external tube skin temperature, K
U = overall heat transfer coefficient, kJ/(m^2 · h · K)
u_s = superficial velocity, m^3_f/(m^2_r · h)
V = volume of catalyst pellet, m^3
V_g = volume of voids in a gram of catalyst mL/g_{cat}
$V_{g,i}$ = volume of void with pore radius $r_i < r < r_{i+1}$ in a gram of catalyst, mL/g_{cat}
$V(i)$ = exponential of reaction affinity, defined by

$$\left(\prod_j p_j^{\nu_j}\right)\Big/ K_i$$

W = amount of catalyst in the reactor, kg
x = distance from surface of catalyst onwards
x_{CH_4} = conversion of CH_4
x_{CO_2} = conversion of CH_4 into CO_2
x'_{CH_4} = conversion of CO_2 into CH_4 when CO_2 and H_2 are fed
x'_{CO_2} = total conversion of CO_2 in reverse of water gas shift
$\hat{x}_j$ = estimated value of x_j
z = reactor coordinate, m

Greek letters

α_i = convective heat transfer coefficient in packed bed, kJ/(m^2 · h · K)
η_{CH_4} = effectiveness factor for methane disappearance
η_{CO_2} = effectiveness factor for CO_2 formation
η_i = effectiveness factor of reaction i, i = I, II, III
η'_1, η'_2, η'_3 = effectiveness factors of the reverse of reactions I, II, III
ϵ_s = porosity of catalyst particle, m^3_{void}/m^3_{cat}
λ_g = thermal conductivity of the process gas, kJ/(m · h · K)
λ_{st} = thermal conductivity of the tube metal, kJ/(m · h · K)
ρ_B = density of the catalyst bed, kg_{cat}/m^3_r
ρ_g = density of the process gas, kg/m^3_f
ρ_s = density of the catalyst solid, kg_{cat}/m^3_{cat}
ξ = radial position in particle
ζ = CO_2/CH_4 molar feed ratio, $kmol_{CO_2}/kmol_{CH_4}$
τ = tortuosity factor
μ = viscosity of the fluid, kg/(m · s)
Ω = cross section of the reactor, m^2
ν_j = stoichiometric coefficient of component j in reaction i

Literature Cited

Beeckman, J., and G. F. Froment, "Deactivation of Catalysts by Coke Formation in the Presence of Internal Diffusional Limitation," *Ind. Eng. Chem. Fund.*, **11**, 242 (1982).

Brauer, H., "Druckverlust in Füllkörpersaülen Bei Einphasen-Strömung," *Chem. Ing. Techn.*, **29**(12), 785 (1957).

De Deken, J., E. F. Devos, and G. F. Froment, "Steam Reforming of Natural Gas: Intrinsic Kinetics, Diffusional Influences and Reactor Design," *Chem. React. Eng., ACS Symp. Ser.*, 196, Boston (1982).

De Wasch, A. P., and G. F. Froment, "Heat Transfer in Packed Beds," *Chem. Eng. Sci.*, **27**, 567 (1972).

Dumez, F. J., and G. F. Froment, "Dehydrogenation of 1-Butene into Butadiene. Kinetics, Catalyst Coking, and Reactor Design," *Ind. Eng. Chem. Proc. Des. Dev.*, **15**(2), 291 (1976).

Ergun, S., "Fluid Flow through Packed Columns," *Chem. Eng. Prog.*, **48**(2), 89 (1952).

Feng, C., and W. Steward, "Practical Models for Isothermal Diffusion and Flow of Gases in Porous Solids," *Ind. Eng. Chem. Fund.*, **12**, 143 (1973).

Froment, G. F., and K. B. Bischoff, *Chemical Reactor Analysis and Design*, John Wiley, New York (1979).

Johnson, M. L., and W. E. Steward, "Pore Structure and Gaseous Diffusion in Solid Catalysts," *J. Catal.*, **4**, 248 (1965).

Kunii, D., and J. M. Smith, "Heat Transfer Characteristics of Porous Rocks," *AIChE J.*, **6**, 71 (Jan., 1960).

Leva, M., "Fluid Flow through Packed Beds," *Chem. Eng.*, **56**, 115 (1949).

Rao, M. V. R., P. M. Plehiers, and G. F. Froment, "The Coupled Simulation of Heat Transfer and Reaction in a Pyrolysis Furnace," *Chem. Eng. Sci.*, **43**(6), 1223 (1988).

Reichelt, W., and E. Blasz, "Strömungstechnische Untersuchungen an mit Raschig-Ringen Gefüllten Füllkörperrohren und Saülen," *Chem. Ing. Techn.*, **43**, 949 (1971).

Van Deemter, J., F. Zuiderweg, and I. Klinkenberg, "Longitudinal Diffusion and Resistance to Mass Transfer as Causes of Nonideality in Chromatography," *Chem. Eng. Sci.*, **5**, 271 (1956).

Wakao, N., and J. Smith, "Diffusion in Catalyst Pellets," *Chem. Eng. Sci.*, **17**, 825 (1962).

Wheeler, A., "Reaction Rates and Selectivity in Catalyst Pores," *Adv. Cat.*, **3**, 248 (1951).

Wilke, C. R., and P. Chang, "Correlation of Diffusion Coefficients in Dilute Solutions," *AIChE J.*, **1**, 264 (Mar., 1955).

Manuscript received Feb. 29, 1988, and revision received Sept. 2, 1988.